20th Australasian Fluid Mechanics Conference
Perth, Australia
5-8 December 2016

Leading edge interfacial phenomena of sheet and cloud cavitation

D. R. Giosio[1], P. S. Russell[1], B. W. Pearce[1] and P. A. Brandner[1]

[1]Cavitation Research Laboratory, Australian Maritime College
University of Tasmania, Tasmania 7250, Australia

Abstract

The formation and dynamics of cavity leading edge cell-like structures on a NACA 16-029 section hydrofoil have been investigated for a range of Reynolds numbers for stable (supercavitation) and shedding cavities (cloud cavitation). Optical measurements of the cavitating structures are made to quantify geometric properties including the size range and shape of the so-called cells, as well as the dynamic behaviour involving growth, division, decline and elimination. Leading edge cell structure was found to be in a state of dynamic equilibrium for the supercavitating case with cell mean cell size a function of the overlying boundary layer thickness. For shedding cavities, the leading edge evolved cyclically from surface related nuclei into streaks, merging to form a contiguous, shedding modulated, cellular structure. In both cases cells grow and with the onset of destabilization division occurs, indicative of the Saffman-Talyor instability.

Introduction

Attached cavitation remains an active area of research in hydrodynamic flows where it may cause performance reduction, and particularly if unsteady in character, also vibration, noise and erosion. The physical mechanisms involved in cavity formation, detachment and condensation of shed vaporous structures, typically termed 'clouds' or 'cloud cavitation', are yet to be adequately explained. These may involve various phenomena including free and surface nucleation, surface energy effects and cavity interfacial instabilities, cavity/boundary layer interaction, laminar to turbulent transition, large-scale turbulence, re-entrant jet formation and shockwave formation.

It is understood that for an attached cavity to form on the surface of a body it is dependent on the existence of laminar boundary layer separation upstream of the cavity, with the distance between the two dependent on Reynolds number [1]. This is supported by the presence of a cellular laminar region at the cavity leading edge which has been observed on axisymmetric head forms [5] , spheres [4, 10] and hydrofoils [8, 9]. In particular, observations on the formation and dynamic behaviour of the laminar cells have been noted in the investigations involving attached cavitation about a sphere with Brandner et al. [4] observing that the cells appeared to be nucleated either from small bubbles adjacent to the surface (remnant from the previous shedding cycle) or from sites on the surface itself. They grow initially from individual bubbles into elongated streaks, eventually forming laminar cells at the leading edge of a part or complete circumferentially attached cavity. This is in contrast to free microbubbles further out in the flow that, when present, are observed instead to be activated as 'travelling bubble' type cavitation which prevent the formation of attached cavitation with the associated leading edge laminar cells [6]. Brandner et al. [4] also discuss the complex interaction between surface nucleation, the overlying boundary layer and the formation and modulation of cell width/splitting and merging with shedding cycles.

As a further contribution to understanding the mechanisms involved in the formation of an attached cavity, and the influence of the leading edge on cavity shedding behaviour or vice versa, an experiment has been conceived using a hydrofoil section with pressure distribution favourable to the formation of an attached cavity. The hydrofoil section has a favourable pressure gradient maintaining laminar flow followed by an unfavourable gradient inducing separation of the upstream laminar boundary layer at 60% chord with subsequent cavity detachment. Data is presented from both High-resolution and high-speed photography for a range of cavitation numbers from inception through to the supercavitating regime. The effect of Reynolds number on leading edge topology and dynamic behaviour has also been examined.

Experimental Setup

Experiments were carried out in the Cavitation Research Laboratory (CRL) variable pressure water tunnel at the Australian Maritime College. The tunnel test section is 0.6 m square by 2.6 m long in which the operating velocity and pressure ranges are 2 to 12 ms^{-1} and 4 to 400 kPa absolute, respectively. The tunnel volume is 365 m^3, which is filled with demineralised water (conductivity of order 1 μS/cm).

The tunnel has ancillary systems for rapid degassing and for continuous injection and removal of nuclei and large volumes of incondensable gas. The test section velocity is measured from one of two (low and high range) Siemens Sitrans P differential pressure transducers (measuring the calibrated contraction differential pressure) with estimated precision of 0.007 ms^{-1} and 0.018 ms^{-1}, respectively. The velocity and pressure in the test section are controlled to maintain a constant Re and σ. The test section velocity is spatially uniform to within $\pm 0.5\%$, has temporal variations of less than 0.2%, and the free stream turbulent intensity is about 0.5%. Detailed descriptions of the facility are given in [2, 3] and [7].

A stainless steel hydrofoil was mounted on the test section ceiling centreline, 1.15 m downstream from the entrance. The hydrofoil geometry consisted of a rectangular planform NACA 16-029 section, with a span of 250 mm, and a chord length of 140 mm.

High-resolution (36.3 megapixel) still photographs were captured using a Nikon D800E DSLR with a Nikon AF-S Micro Nikkor 105 mm 1:2.8G ED lens. Illumination was provided by two simultaneously triggered stroboscopes, a Drello 3018 scope with 4037 flashlamp and a Drello 1018 scope with 4040 flashlamp. High-speed photographic images were acquired at 3,000 Hz using a LaVision HighSpeedStar5 CMOS 10-bit 1 megapixel camera with a Nikon AF Nikkor 50 mm 1:1.8D lens. A combination of high powered LED light units including 2 custom-made lamps (based on the Cree XLamp CXA3050 LED) and a Veritas Constellation 120 W light source were used to obtain sufficient illumination.

Experimental Procedure

All data were obtained at zero incidence for three chord-based

Reynolds numbers, $Re_c = Uc/\nu$, of 0.8, 1.2 and 1.6 $\times 10^6$ (where U is the free stream velocity, c the chord length and ν the kinematic viscosity). Two cavitating regimes were investigated – periodic shedding and stable supercavity – corresponding to cavitation numbers, $\sigma = (p - p_v)/(\frac{1}{2}\rho U^2)$, of 0.52 and 0.25, respectively (where p is the freestream static pressure at the mid-span of the hydrofoil, p_v the vapour pressure, and ρ the density of the fluid). The dissolved oxygen content was maintained between 2.5 and 3 ppm for all test conditions.

For each test condition 200 still images were captured for cavity leading edge cell size determination. In separate runs, 2048 frames were captured at each condition using the high-speed set-up for investigation of cavity cell development.

Results and Discussion

Image processing of both high-resolution, and high-speed images were performed in MATLAB to investigate the geometry of the cavity leading edge with Re and σ. Each image was processed with a reconstruction-based opening and closing routine before a locally adaptive threshold was applied. The leading edge was detected by sampling pixel intensities in the laminar region of the cavity leading edge as shown in Figure 1. Further sampling was performed to weight probable cell boundaries followed by peak detection to then determine the spanwise cell widths.

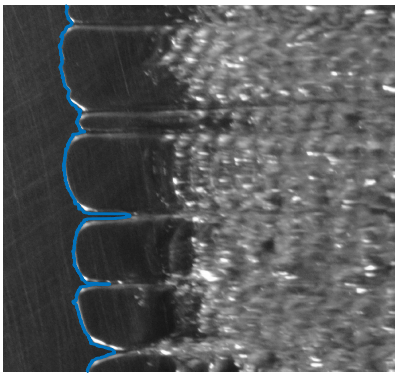

Figure 1: Results of image processing to detect the cavity leading edge. Test conditions $Re = 1.6 \times 10^6$, $\sigma = 0.25$.

Non-dimensional mean span-wise cell widths, s/c, presented in Figure 2 as a function of Reynolds number, were determined from high-resolution images under supercavitating conditions ($\sigma = 0.25$) such that the cavity was stable and non-shedding. Examples of processed images at each of the three test Reynolds numbers are shown in Figure 3 with the coloured bars demarcating the individual detected cell widths. As evidenced in Figures 2 & 3 the mean cell width is shown to decrease with increasing Reynolds number at constant σ. This behaviour suggests a potential interaction between the detaching cavity and secondary flows in the separating, destabilised boundary layer. While the presence of the cavity and the streamwise location of the cavity leading edge was stable, the cells themselves are in a state of dynamic equilibrium undergoing growth, division, decline and elimination as larger cells preferentially increase in width forcing the declining cells to be washed downstream. Additionally, a general downward (spanwise) movement was observed although local cell movement may be upwards. The cell division occurs follow a destabilisation of the cavity leading edge suggesting a Saffman-Taylor type instability.

The same cell detection routine was applied to the high-speed images at the higher cavitation number, σ = 0.52, to examine the cycle of cavity leading edge formation, growth and extinction by re-entrant jet formation and subsequent shockwave initiation. Shedding frequencies were calculated to be 23.44 Hz, 33.69 Hz, and 45.41 Hz for the three test Reynold numbers of 0.8×10^6, 1.2×10^6, and 1.6×10^6, respectively, corresponding to a constant test Strouhal number of $\sim$0.15.

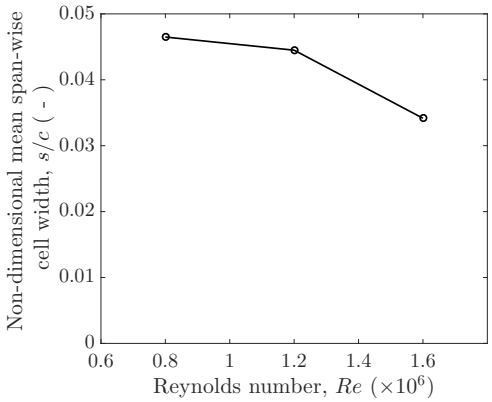

Figure 2: Mean leading edge cavity cell width, non-dimensionalised by chord length, as a function of Reynolds number under supercavitating conditions (σ = 0.25).

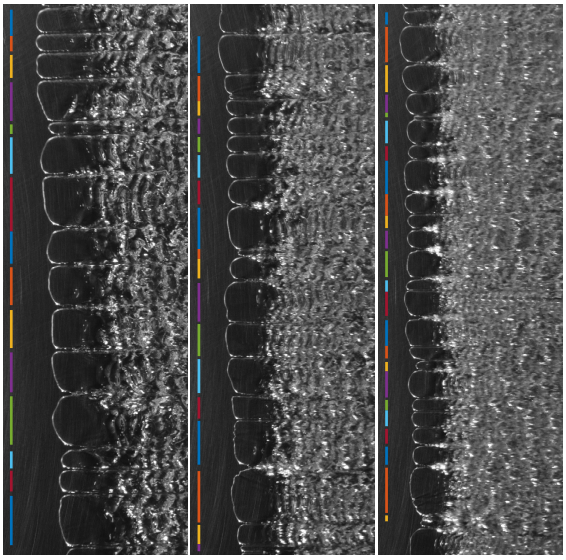

(i) 0.8×10^6 (ii) 1.2×10^6 (iii) 1.6×10^6

Figure 3: Cavitation leading edge cell detection on a NACA 16-029 section hydrofoil as a function of Reynolds number. All tests performed at a cavitation number of σ = 0.25 under supercavitating conditions.

For shedding cavities the leading edge structure evolved cyclically from small remnant cavities or surface nuclei forming streaks that merge to form a contiguous cavity but retain a cellular structure. A full cycle is shown in Figure 4 at a Reynolds number of 0.8×10^6. Mean spanwise cell widths as a function of time are plotted across multiple cycles in Figure 5 for the three investigated Reynolds numbers. The temporal location of images (i) - (x) in Figure 4 are indicated by circular markers. In each case the mean spanwise cavity cell width can be seen to increase across a cycle, with cavity growth, until the shockwave, initiated by the re-entrant jet, reaches the cavity leading edge (Figure 4(iv)).

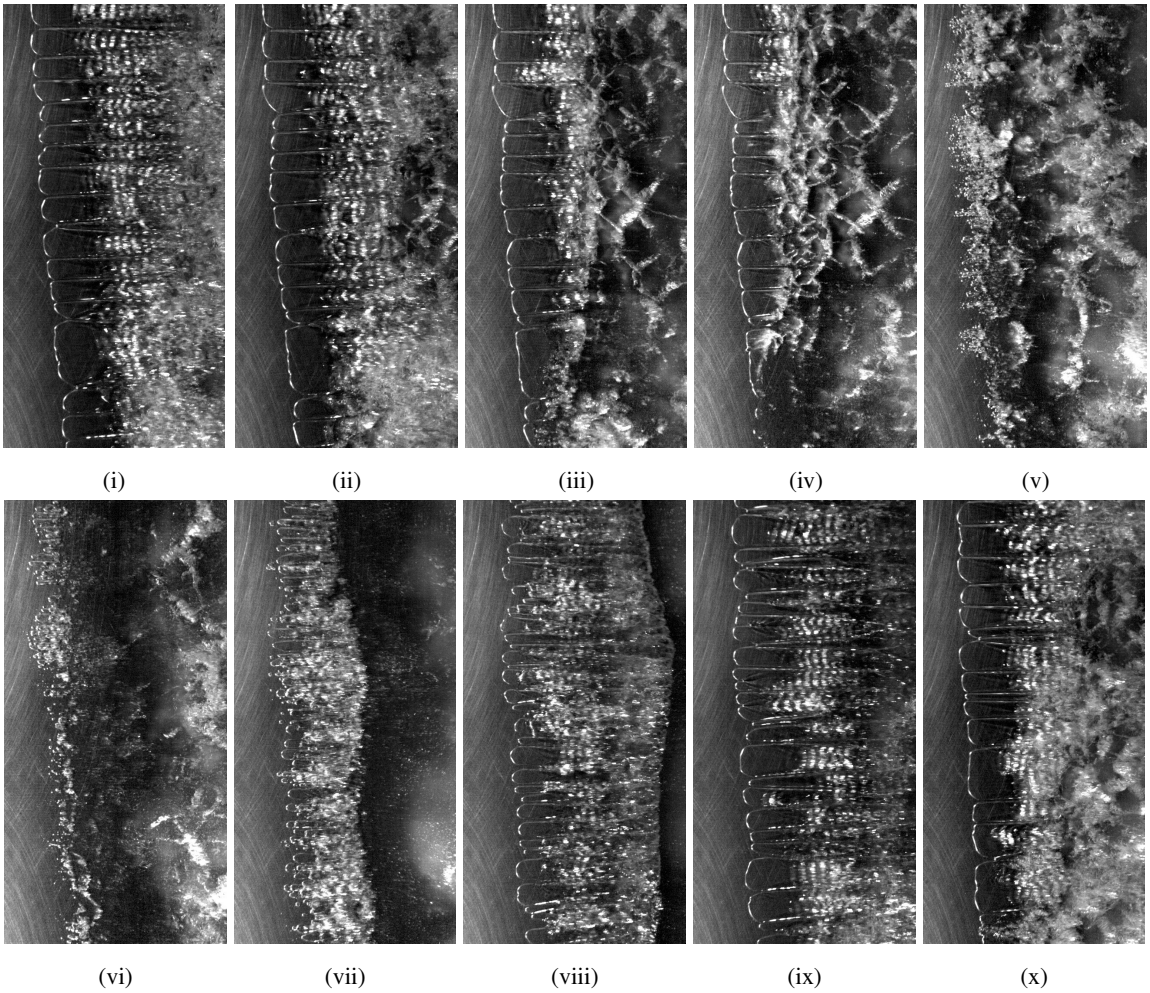

Figure 4: Selected frames over one full shedding cycle taken from a high-speed recording at a test condition of $Re = 0.8 \times 10^6$, $\sigma = 0.25$.

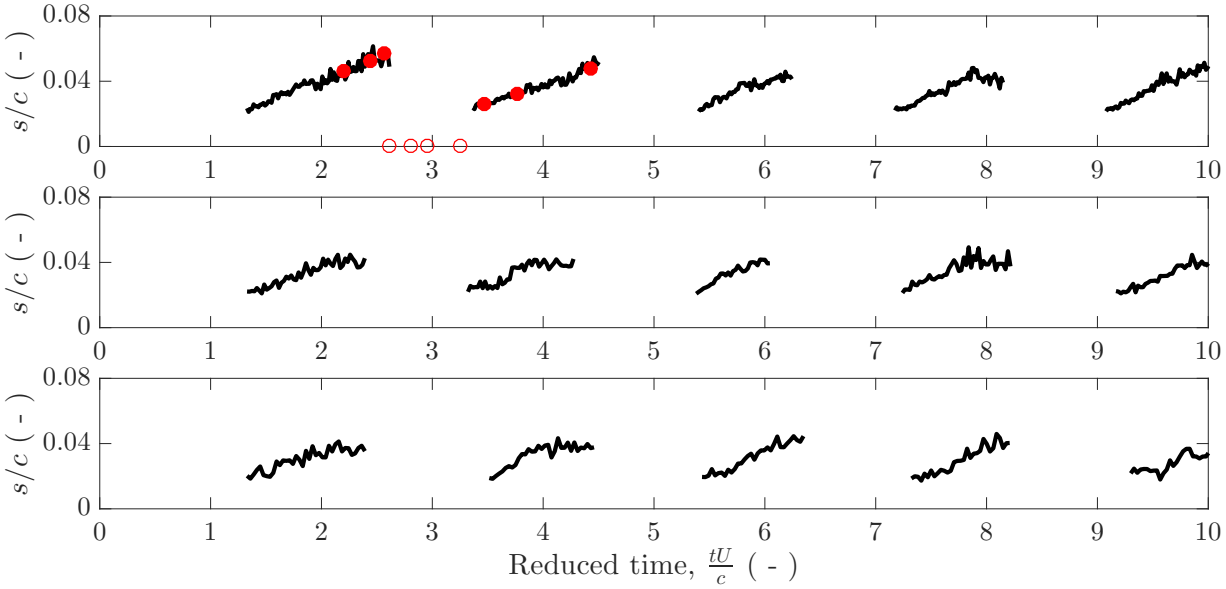

Figure 5: Mean leading edge cavity cell width during the growth phase of the shedding cycle at a cavitation number of $\sigma = 0.52$ for Re = 0.8×10^6 (top), Re = 1.2×10^6 (middle), Re = 1.6×10^6 (bottom). Red markers on the top plot correspond to images (i) - (x) in Figure 4 (hollow markers indicate that no cell size data was calculated).

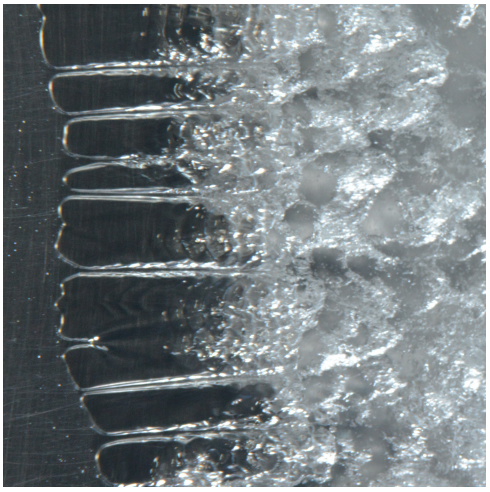

Figure 6: Remnant vapour cavities upstream of the cavity leading edge toward the end of a shedding cycle at a test condition of $Re = 0.8 \times 10^6$, $\sigma = 0.52$.

The breakup of the laminar cells by the shockwave produces tiny remnant volumes of vapour that are transported upstream of the previous cavity leading edge position. These remnant volumes may provide sites for cavity renewal, however, a significant number also remain trapped in the separation bubble ahead of the newly formed cavity as seen in Figure 6. During the cycle the streamwise and spanwise position of these remnant bubbles seem to be modulated by/associated with the movement of the adjacent cell and remain upstream of the cavity proper, however, occasionally they can be seen to be rapidly transported downstream, impacting on the surface of the laminar cell. Two such instances of this can been seen in the lower half of Figures 4(ix) & 4(x) as surface disturbances on the laminar surface of the cavity cell.

Conclusions

The formation and dynamics of cavity leading edge cell-like structures on a NACA 16-029 section hydrofoil has been investigated for a range of Reynolds numbers at cavitation numbers of 0.25 and 0.52 creating stable (super), and shedding (cloud) cavitation, respectively.

Leading edge cell structure was found to be in a state of dynamic equilibrium for the supercavitating case. In this case the average cell size has been shown to be a function of the Reynolds number and hence the overlying boundary layer thickness. This behaviour suggests a potential interaction between the detaching cavity and secondary flows in the separating, destabilised boundary layer.

For shedding cavities the leading edge structure evolved cyclically, from small remnant cavities or surface nuclei, forming streaks that merge to form a contiguous cavity but retain a cellular structure. The width of the cells are modulated with the shedding cycle, with the mean width increasing during the cavity growth phase where the boundary layer is accelerating and is presumably more stable. During the growth cycle some cells preferentially increase in width, while others necessarily reduce.

Just prior to cell division occurring the cavity leading edge appears to become unstable suggesting possible Saffman-Taylor instability. As indicated by the observed dependence of mean cell width on Reynolds number the interaction with the overlying boundary layer of varying thickness and stability is possibly playing a role in the cell behaviour.

Acknowledgements

This work has been supported by the Australian Maritime College, the Defence Science and Technology Group, Australian Department of Defence, and the US Office of Naval Research.

References

[1] Arakeri, V. H., Viscous effects on the position of cavitation separation from smooth bodies, *Journal of Fluid Mechanics*, **68**, 1975, 779–799.

[2] Brandner, P. A., Lecoffre, Y. and Walker, G. J., Development of an Australian National Facility for Cavitation Research, in *Sixth International Symposium on Cavitation CAV2006*, 2006.

[3] Brandner, P. A., Lecoffre, Y. and Walker, G. J., Design Considerations in the Development of a Modern Cavitation Tunnel, in *16th Australasian Fluid Mechanics Conference*, 2007.

[4] Brandner, P. A., Walker, G. J., Niekamp, P. N. and Anderson, B., An experimental investigation of cloud cavitation about a sphere, *Journal of Fluid Mechanics*, **656**, 2010*a*, 147–176.

[5] Ceccio, S. and Brennen, C., Dynamics of attached cavities on bodies of revolution, *Journal of Fluids Engineering*, **114**, 1992, 93–99.

[6] de Graaf, K. L., Pearce, B. W. and Brandner, P., The influence of nucleation on cloud cavitation about a sphere, in *ISROMAC16 - Sixteenth International Symposium on Transport Phenomena and Dynamics of Rotating Machinery*, 2016.

[7] Doolan, C., Brandner, P., Butler, D., Pearce, B., Moreau, D. and Brooks, L., Hydroacoustic characterisation of the AMC cavitation tunnel, in *Acoustics 2013 - Science, Technology and Amenity*, Victor Harbour, Australia, 2013.

[8] Farhat, M., Guennoun, F. and Avellan, F., The leading edge cavitation dynamics, in *ASME 2002 Fluids Engineering Division Summer Meeting*.

[9] Franc, J. and Michel, J., Attached cavitation and the boundary layer: experimental investigation and numerical treatment, *Journal of Fluid Mechanics*, **154**, 1985, 63–90.

[10] Tassin Leger, A., Bernal, L. and Ceccio, S., Examination of the flow near the leading edge of attached cavitation: Part 2. incipient breakdown of two-dimensional and axisymmetric cavities, *Journal of Fluid Mechanics*, **376**, 1998, 91–113.